Joint qualitative and quantitative evaluation of fast image dehazing based on dark channel prior

Aksas, Lyes, Lapray, Pierre-Jean, Foulonneau, Alban, Bigué, Laurent

SPIE.

Joint qualitative and quantitative evaluation of fast image dehazing based on dark channel prior

Lyes Aksas[a], Pierre-Jean Lapray[a], Alban Foulonneau[a], and Laurent Bigué[a]

[a]IRIMAS, EA7499, Université de Haute-Alsace, Mulhouse, France

ABSTRACT

Haze is an undesirable effect in images caused when atmospheric particles, such as water droplets, ice crystals, dust, or smoke, are lit directly or indirectly by the sun. This effect can be counteracted by image processing, to bring back the details of a hazy image. Unfortunately, the execution time is often long, which prevents deployment in some video or real-time applications. In this paper, we propose to tune several parameters of the Dark Channel Prior method (DCP) algorithm combined with the fast guided filter. We evaluate the optimization in terms of execution time, and quantify the output image quality using different image quality metrics.

Keywords: Dehazing; Dark Channel Prior; Optimization; algorithm acceleration

1. INTRODUCTION

Atmospheric haze is a source of image degradation, which is produced by the scattering of particles. This effect can be counteracted by image processing. Several algorithms have been developed and are categorized as either prior-based methods,[1–3] or learning methods.[4,5] The former are intended to inverse a physical model using prior assumptions on the scattering effect, whereas the latter use training data to elaborate a black box. Another group of methods is based on image enhancement.[6–8]

The execution times of dehazing algorithms are often high and can rise dramatically with the image resolution. This avoids such kind of algorithms to be implemented in real-time video applications such as image-guided robotics, welding process, tracking, or remote sensing.Nevertheless, Artusi *et al.*[9] compared several haze removal techniques in a recent survey, looking at their computational efficiency. They classified the dehazing algorithms in two different groups, 1-the high computational cost methods,[10–13] and 2-the low computational cost methods.[12,14–16] They found that, among all the prior-based methods, the Dark Channel Prior (DCP) method provides the best overall quality performance over the selected metrics and dataset. Moreover, its optimized version, namely the Dark Channel Prior Fast (DCPF), turns out to be one of the fastest methods in terms of computation time.[9]
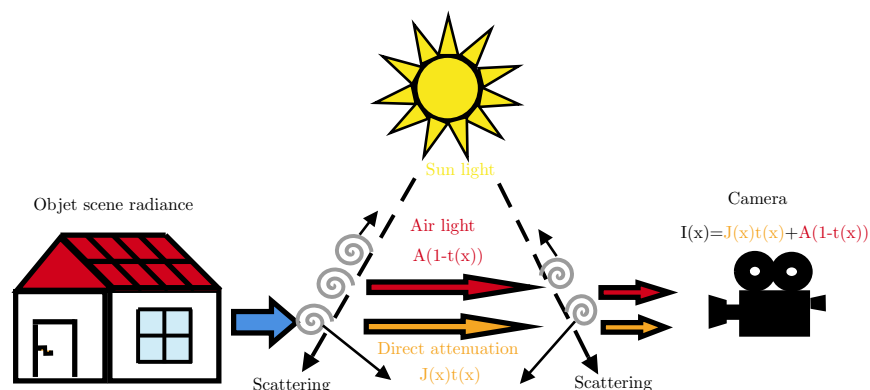

Figure 1. Imaging of a scene through haze. The illumination is scattered by the atmospheric particles and acts as an additive intensity component to the object radiance.

Further author information: Lyes AKSAS: E-mail: lyes.aksas@uha.fr

This article proposes to tune the parameters of the DCPF method for an optimization purpose, and to quantify the image quality results accordingly. The paper is organized as follows. In Section 2, we first describe the different processing steps of the Dark Channel Prior algorithm and its optimization through DCPF. We then describe the optimization parameters. We build the experiment in Section 3, before the results and discussing them in Section 4. Finally, the conclusion is given in Section 5.

2. BACKGROUND

2.1 Dark Channel Prior

The Dark Channel Prior method is an efficient physics-based algorithm for haze removal, proposed by He *et al.*[3,12] It is inspired by the Koschmeider model,[17] where the radiance that reaches the sensor results from a contribution from the object in the scene and the atmospheric light. This gives the following additive model:

$$\mathbf{I}(x) = \mathbf{J}(x).t(x) + \mathbf{A}.[1 - t(x)] \ , \tag{1}$$

where x refers to the pixel position, $\mathbf{I}(x)$ is the observed image intensities, $\mathbf{J}(x)$ is the scene radiance, $\mathbf{A}$ is the atmospheric light (airlight), and $t(x)$ is the transmission that defines how the light is traversing the air. A haze-free image will typically result from a transmission equal to one (no airlight component). The scattering effect is schematically depicted in Figure 1.
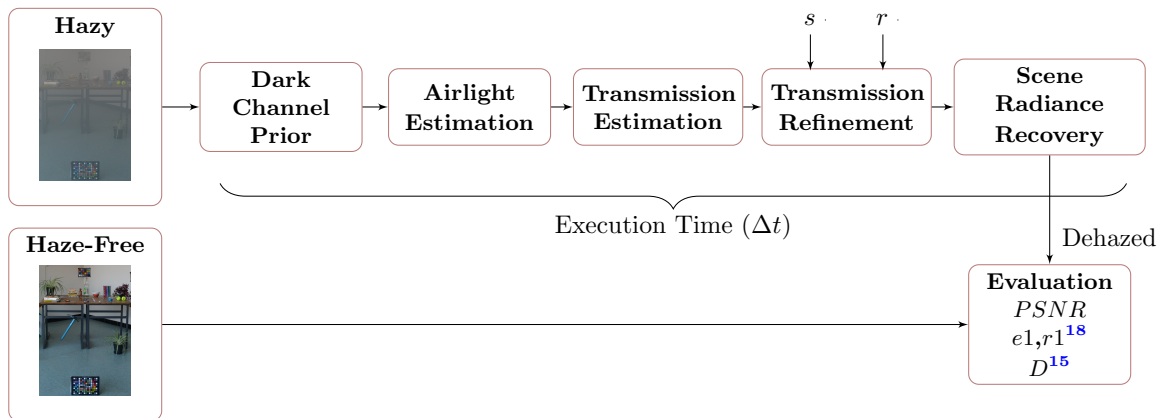

Figure 2. Experimental pipeline used in this work. The sampling factor s and the radius r are the parameters which are made variable.

To inverse the model in Equation 1, we recover $\mathbf{J}$ from the estimation of $t(x)$ and $\mathbf{A}$. To this end, the DCP algorithm consists of by five sub-processing steps, which are summarized in Figure 2. We describe the five steps in the following.

1. Dark Channel Prior

   The principal assumption of the DCP algorithm comes from the dark channel concept. This is a discovery based on a statistical observation: in a haze-free image, the minimum of intensities among all color components and within a small area of pixels is always close to zero. Thus, the dark channel is computed as:

$$I^{dark}(\mathbf{x}) = \min_{\mathbf{y} \in \Omega(\mathbf{x})} \left(\min_{c \in (r,g,b)} \left(I^c(\mathbf{y}) \right) \right) \ , \tag{2}$$

   where I^{dark} is the dark channel, I^c is the intensity in spectral channel c, and $\Omega(\mathbf{x})$ is a local patch centered at position x. An example of the dark channel results is illustrated in Figure 4, where the computation is done for both a haze-free and a hazy image.

2. Airlight Estimation

The airlight $\mathbf{A}$ is the additional component in the presence of haze. This is estimated following the assumption that, at infinite distance ($t \approx 0$), the brightest intensity is the most haze-opaque element from the scene, and it approximately equals $\mathbf{A}$. It is practically computed in two steps: 1-find the 0.1% of the brightest pixels in the dark channel, and 2-find the highest intensity pixel in $\mathbf{I}$ from the region made of the 0.1% of the brightest pixels in the dark channel. The three RGB airlight components for the hazy image in Figure 4 are [0.767, 0.768, 0.760].

3. Transmission Estimation

The estimation of the transmission at each pixel position is computed from the dark channel and the estimated airlight such as:

$$\hat{t}(\mathbf{x}) = 1 - \omega \min_{\mathbf{y} \in \Omega(\mathbf{x})} \left(\min_{c \in (r,g,b)} \left(\frac{I^c(\mathbf{y})}{A^c} \right) \right) , \tag{3}$$

where $\omega = 0.95$ permits to keep a small amount of haze for the distant objects and avoid unnaturalness of image.

4. Transmission Refinement

As the transmission map is computed from the dark channel, and that the dark channel value is computed patchwise, the transmission map suffers from a loss of high spatial frequencies. To restore the edges in the transmission map, we need to refine the transmission map. It is done by using a soft matting Laplacian[3, 19] to smooth artifacts and reconstruct the edges in the transmission map.

5. Scene Radiance Recovery

Finally, the radiance is computed from the refined transmission map, the airlight, and the input image as follows:

$$\mathbf{J}(\mathbf{x}) = \frac{\mathbf{I}(\mathbf{x}) - \mathbf{A}}{\max(t(\mathbf{x}), t_0)} + \mathbf{A} , \tag{4}$$

where a lower bound $t_0 = 0.1$ permits to mitigate the noise in case of very low transmission.

2.2 Dark Channel Prior Fast (DCPF)

2.2.1 Dark Channel Prior with Guided Filter

An optimized version of DCP has been proposed by the DCP authors themselves:[20] the soft matting used to refine the transmission map (step 4) is substituted by a guided image filtering, where the input image $\mathbf{I}$ is used as the guide. This filtering is based on a local computation of two linear coefficients, in such a way that it minimizes the reconstruction error between the input and the guidance data. The radius of the filter window is noted r. This method is fast and has the smoothing capabilities, such as the bilateral filtering, without suffering from gradient inversion artifacts.

2.2.2 Dark Channel Prior with Fast Guided Filter

In addition, an optimization of the guided image filtering has been proposed to dramatically reduce the execution time.[13] In fact, they realize that the major computation time is dedicated to the linear coefficient maps. But a full resolution image is not needed at this stage. Thus, to optimize computationally, they propose to reduce the resolution during the refinement step. A simple bilinear subsampling of both the input and the guidance images is performed prior to the guided filtering. Once the coefficient are computed, an upsampling of these is done. This ensures that the refined transmission map keeps the initial spatial resolution. The subsampling/upsampling factor is noted s.

2.3 Optimization strategies

We want to identify the steps of the algorithm which are the most time-consuming. To this end, we implement the DCPF with guided filter (with $r = 32$ and $s = 4$), and use an image resolution of 2444×1566. We obtain the diagram in Figure 3(a). It appears that the refinement is the most time-consuming step. This seems judicious to make the sampling factor s and the radius r variables. We propose to jointly evaluate these parameters relatively to the image quality and the execution time. It is also interesting to evaluate when keeping the ratio $r_p = \frac{r}{s}$ constant, as it was done in.[13]
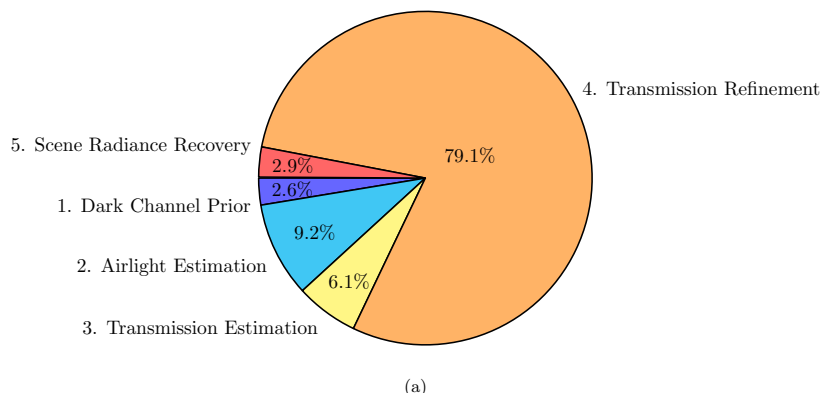

(a)

Figure 3. Execution time of the DCPF algorithms using a radius $r = 32$, a sampling factor $s = 4$, a patch size of 59,

3. EXPERIMENT

We run the DCPF[12][13] algorithm with Matlab 2020b on a computer with an Intel(R) Core(TM) i7-6700 CPU @ 3.40 GHz, 16.0 Go of DDRAM, on Windows 10 64-bit operating system.

3.1 Image Data

We select two images from the CHIC database[21,22] (Color Hazy Image for Comparison): a haze-free image (named "*Scene1_IM_Level10(without_fog)*") which will serve as a reference, and a hazy image (named "*Scene1_IM_Level5*").
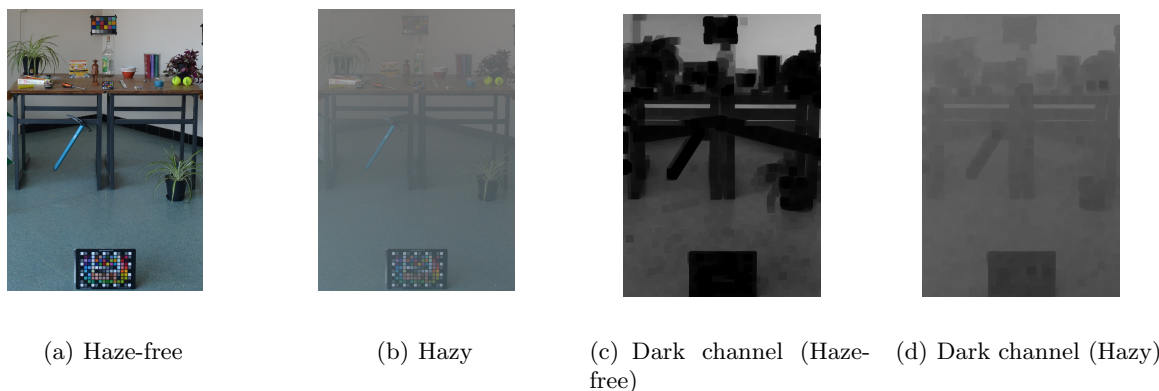

(a) Haze-free   (b) Hazy   (c) Dark channel (Haze-free)   (d) Dark channel (Hazy)

Figure 4. (a)-(b) The two images used for the evaluation. Both images come from the CHIC dataset.[21,22] The size of the images is 2244×1566 pixels. (c)-(d) The corresponding dark channel images computed with the algorithm from He *et al.*[12] The airlight estimates are (a): $\mathbf{A}$=[0.706,0.710, 0.717], and (b): $\mathbf{A}$=[0.520,0.516, 0.509],

3.2 Metrics

The results are quantitatively evaluated through three different quality metrics:

- Execution time (dt) of the dehazing algorithm, which includes the five steps presented in Section 2.

- PSNR (Peak Signal to Noise Ratio), as an objective quality metric which is not dedicated to dehazing.

- Hautière et al.[18] which measures the improvement in the visibility of edges before and after dehazing. Two parameters are given by the metric: $e1$ and $r1$. The rate of new visible edges is depicted as $e1$, whereas the restoration quality (geometric mean ratios of visible gradients) is $r1$. The parameter $r1$ takes into account both visible and non-visible edges. Two input images (hazy and dehazed) are needed to assess the restoration quality. Higher $e1$ or $r1$ values mean better performance in contrast restoration.

- FADE[15] (Fog Aware Density Evaluator) which is a referenceless metric based on Natural Scene Statistics (NSS) and fog aware statistical features. The output D is computed on a single image and gives a low value for a low fog perception.

4. RESULTS AND DISCUSSION

We propose to visualize the metric results for three scenarios, which forms three groups of metric results:

1. Results with r kept constant (only s varies), Figure 5.

2. Results with s kept constant (only r varies), Figure 6.

3. Results with the ratio $r_p = \frac{r}{s}$ kept constant (r and s vary together), Figure 7.

The fixed values of s and r for the two first scenario are chosen as it is defined in the Matlab implementation (function 'imreducehaze', with 'approxdcp' method option), i.e. $s = 4$ and $r = 32$. The patch size for Ω is fixed to 59 (as in the Matlab implementation for this image resolution).

4.1 Influence of s

(a) Execution time   (b) New visible edge   (c) Quality of restoration
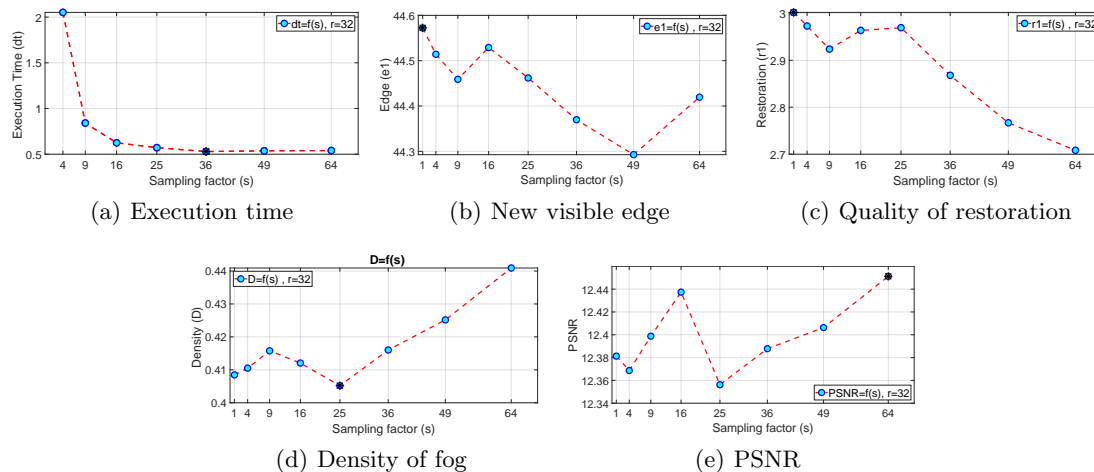
(d) Density of fog   (e) PSNR

Figure 5. Metric results when the radius r is kept constant. Black cross represents the best dehazed image for the considered metric in the set of tested combinations.

Figure 5 shows the metric results when varying only the sampling factor. Black crosses indicate the best dehazed images by metric and in the set of tested cases. Figure 5(a) shows the execution time as a function of the sampling factor s. For best visualization, we omit the case $s = 1$ where we got $dt = 25.94s$. Globally, we can see

that dt decreases exponentially with the sampling factor. This is somehow intuitive, as resizing the transmission map before refinement makes the filtering operation faster (it operates on a smaller amount of data). After $s = 36$, the s parameter has little impact on the execution time.

From Figure 5(b)-5(e), we see that the amplitude of metric values is very low compared to those of Figure 6. The trends seem not significant when we change the parameter value. This means that, for a constant radius, the sampling factor has low impact on the quality of dehazed images.

4.2 Influence of r

(a) Execution time   (b) New visible edge   (c) Quality of restoration
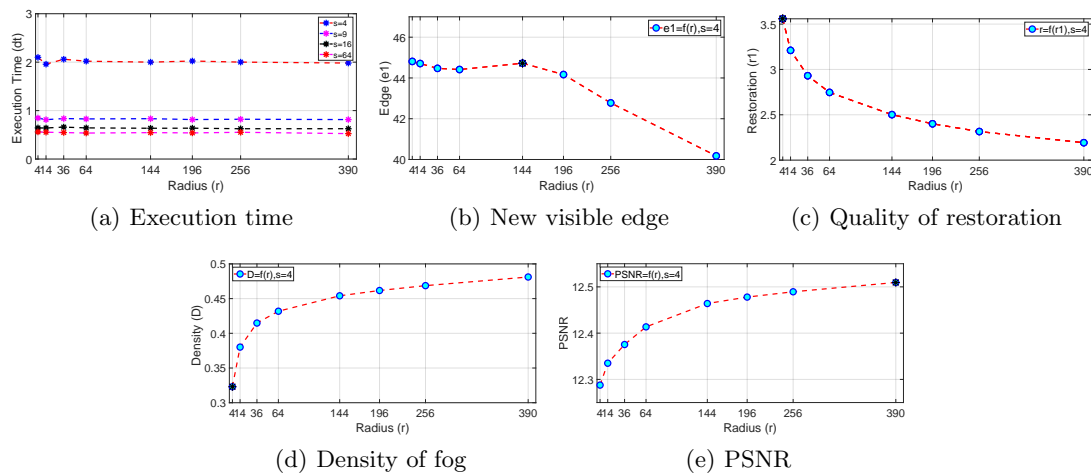
(d) Density of fog   (e) PSNR

Figure 6. Metric results when the sampling factor s is kept constant.

From Figure 6(a), we can deduce that the radius has not impact on the execution time dt. This was expected as it is stated in He *et al.*,[13] where they stated that the guided filter process is $O(N)$ time, and thus, independent of the window radius r and the intensity range. It is to note that with this architecture configuration, the achievable framerate for $s = 4$ is $0.5 fps$, and increases from $1.6 fps$ with $s = 16$ to $1.85 fps$ with $s = 64$.

By looking at quality metrics, we see that the radius parameter has much more impact on the final results than s, where the curves have significant trends. In Figure 6(b), we see that the amount of new visible edges decrease after $r = 144$. Contrary, the quality of restoration and the density of fog are getting worst rapidly when the radius increases, and seem to stabilize at high values.

Unlike other metrics, PSNR is slightly improving when the radius increases. But this improvement is so tiny that we can wonder if it is really significant. We can explain this phenomenon by two observations. First, the dehazed images are somehow very dark compared to the reference image, which explains the overall low PSNR values. Secondly, as the density of fog D increases with the radius, the overall luminance in the dehazed image tends to get higher, which globally reduces the mean square error between the dehazed image and the reference, and thus, makes the PSNR higher.

4.3 Influence of r_p

Figure 7 shows the results with the ratio r_p constant between the radius and sampling factor. We fixed $r_p = 4$ as suggested in.[13] From these curves, we observe the same trends as in Figure 6, with no significant improvement in the metric results. This seems to indicate that keeping the ratio r_p constant has no significant impact on the results as compared to varying only r.

4.4 Visualization

Figure 8 shows the best dehazed images by metric among all the cases tested in this paper. Visually, we see very similar results, except for some sharp edges which seem better reconstructed in Figure 8(e).

We also show, in Figure 8(e), the dehazed images when r is low compared to the donwsampled transmission image (i.e. s is high). These cases produce halo artifacts around strong edges. It seems to become more pronounced as r_p becomes small. The halo effect is a known issue for guided filters,[23] which typically comes when radius is low compared to the selected patch size (Ω) in the dark channel step.[24]

(a) Execution time   (b) New visible edge   (c) Quality of restoration
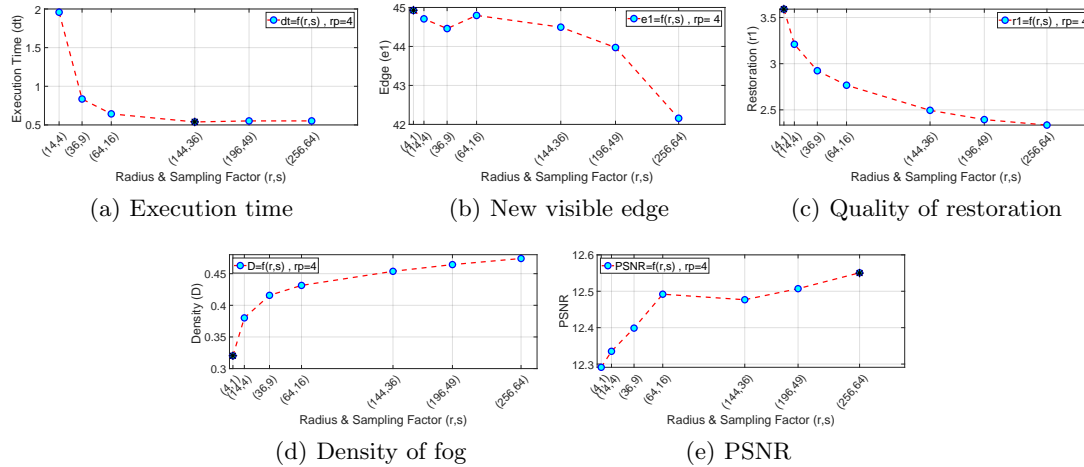
(d) Density of fog   (e) PSNR

Figure 7. Metric results when the ratio r_p is kept constant.

4.5 General remarks

From the above results, we can make several recommendations for the selection of r and s to optimize the dehazing using DCPF: 1-it is necessary to have a high sampling factor for a high framerate, 2- we need to keep the radius as low as possible to have the best quality of restoration/edges and to have a low fog perception in the dehazed image, 3-it is necessary to have a high relative radius r_p compared to the patch size to avoid artifacts around edges. Considering all the remarks above, a good compromise would be to have $s = 36$ and $r = 36$.

We should be careful in interpreting the results of the PSNR metric, even though it is a metric often used in recent review articles. In Figures 6(e) and 7(e), the PSNR evolutions are negatively correlated with the metrics dedicated to dehazing. Thus, it may not reflect the amount of details restored during the dehazing. Evaluation with PSNR seems to be biased by the overall intensity differences between the dehazed image and the reference image: as the fog density reduces the overall intensity difference, the PSNR increases. Nevertheless, this behaviour needs to be investigated more deeply through several reference and hazy images.

All the observations and analysis we made have to be confirmed in the future using a large dataset of images, with different depths of field, and different densities of fog. This can help to robustly confirm the trends of selecting the refinement parameters. The exploration on how to optimize the other steps of the DCPF algorithm before to a practical system implementation is also to be considered.

5. CONCLUSION

This work present a joint evaluation of computational efficiency and quality of dehazed images using the fast dark channel prior method. We studied the impact of two parameters in the refinement step of the algorithm, by testing sixty-four different combinations of radius and sampling factors.

We found that the radius has not an impact in execution time, and low radius gives better metric results. We also found that the sampling factor has a significant impact in the execution time, but has low influence in the quality of restored images. The relative radius r_p needs to be carefully chosen with respect to the patch size to avoid apparition of artifacts. For a patch sier of 59, a good compromise would be $s = 36$ and $r = 36$. These findings need to be confirmed on a large dataset of images.

As a future work, we can study the optimization of other steps of the DCPF algorithm, and implement the algorithm on an efficient hardware architecture.

(a) dt - r= 390, s= 64 (b) (e1, r1, D) - $r = 4, s = 1$ (c) PSNR - $r = 256, s = 64$

(d) dt,r= 390, s= 64 (e) (e1, r1, D) - $r = 4, s = 1$ (f) PSNR - $r = 256, s = 64$
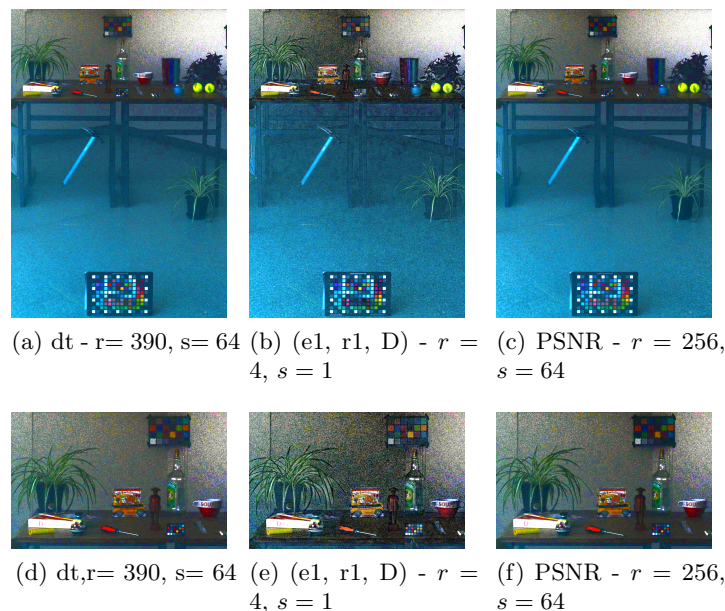
Figure 8. (a)-(c) Visualization of the best dehazed images for each considered metric in the set of tested combinations, and (d)-(f) zoomed versions. A gain of 2 is applied on output dehazed images for visualization purpose.
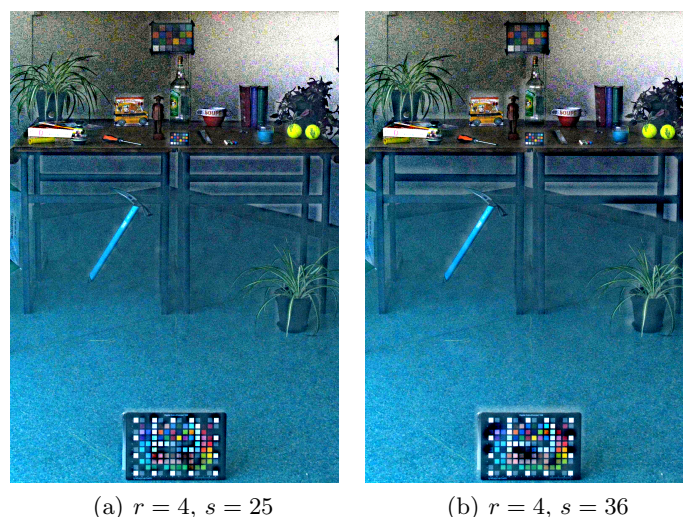

(a) $r = 4$, $s = 25$ (b) $r = 4$, $s = 36$

Figure 9. Visualization of the halo artifacts around edges.

ACKNOWLEDGMENTS

REFERENCES

[1] He, K., Sun, J., and Tang, X., "Single image haze removal using dark channel prior," in [2009 IEEE Conference on Computer Vision and Pattern Recognition], 1956–1963 (2009).

[2] Lapray, P.-J., Thomas, J.-B., and Farup, I., "Bio-inspired multimodal imaging in reduced visibility," Frontiers in Computer Science **3** (2022).

[3] He, K., Sun, J., and Tang, X., "Single image haze removal using dark channel prior," IEEE transactions on pattern analysis and machine intelligence **33**(12), 2341–2353 (2010).

[4] Cai, B., Xu, X., Jia, K., Qing, C., and Tao, D., "Dehazenet: An end-to-end system for single image haze removal," IEEE Transactions on Image Processing **25**(11), 5187–5198 (2016).

[5] Kim, Y. and Yim, C., "Image dehaze method using depth map estimation network based on atmospheric scattering model," in [2020 International Conference on Electronics, Information, and Communication (ICEIC)], 1–3 (2020).

[6] Tarel, J.-P. and Hautière, N., "Fast visibility restoration from a single color or gray level image," in [2009 IEEE 12th International Conference on Computer Vision], 2201–2208 (2009).

[7] Liu, X., Liu, C., Lan, H., and Xie, L., "Dehaze enhancement algorithm based on retinex theory for aerial images combined with dark channel," Open Access Library Journal **7**, 1–12 (2020).

[8] Wang, W. and Yuan, X., "Recent advances in image dehazing," IEEE/CAA Journal of Automatica Sinica **4**(3), 410–436 (2017).

[9] Artusi, A. and Raftopoulos, K. A., "A framework for objective evaluation of single image de-hazing techniques," IEEE Access **9**, 76564–76575 (2021).

[10] Galdran, A., "Image dehazing by artificial multiple-exposure image fusion," Signal Processing **149**, 135–147 (2018).

[11] Meng, G., Wang, Y., Duan, J., Xiang, S., and Pan, C., "Efficient image dehazing with boundary constraint and contextual regularization," in [2013 IEEE International Conference on Computer Vision], 617–624 (2013).

[12] He, K., Sun, J., and Tang, X., "Single image haze removal using dark channel prior," IEEE Transactions on Pattern Analysis and Machine Intelligence **33**(12), 2341–2353 (2011).

[13] He, K. and Sun, J., "Fast guided filter," (2015).

[14] Sulami, M., Glatzer, I., Fattal, R., and Werman, M., "Automatic recovery of the atmospheric light in hazy images," in [2014 IEEE International Conference on Computational Photography (ICCP)], 1–11 (2014).

[15] Choi, L. K., You, J., and Bovik, A. C., "Referenceless prediction of perceptual fog density and perceptual image defogging," IEEE Transactions on Image Processing **24**(11), 3888–3901 (2015).

[16] Chen, C., Do, M. N., and Wang, J., "Robust image and video dehazing with visual artifact suppression via gradient residual minimization," in [ECCV], (2016).

[17] Koschmeider, H., "Theorie der horizontalen sichtweite," Beitrage zur Physik der freien Atmosphare **12**, 33–53 (1924).

[18] Hautière, N., Tarel, J.-P., Aubert, D., and Éric Dumont, "Blind contrast enhancement assessment by gradient ratioing at visible edges," Image Analysis & Stereology **27**(2), 87–95 (2011).

[19] Levin, A., Lischinski, D., and Weiss, Y., "A closed-form solution to natural image matting," IEEE Transactions on Pattern Analysis and Machine Intelligence **30**(2), 228–242 (2008).

[20] He, K., Sun, J., and Tang, X., "Guided image filtering," IEEE Transactions on Pattern Analysis and Machine Intelligence **35**(6), 1397–1409 (2013).

[21] El Khoury, J., Thomas, J.-B., and Mansouri, A., "A color image database for haze model and dehazing methods evaluation," in [Image and Signal Processing], Mansouri, A., Nouboud, F., Chalifour, A., Mammass, D., Meunier, J., and Elmoataz, A., eds., 109–117, Springer International Publishing, Cham (2016).

[22] El Khoury, J., Thomas, J.-B., and Mansouri, A., "A database with reference for image dehazing evaluation," Journal of Imaging Science and Technology **62**(1), 10503–1–10503–13 (2018).

[23] He, K., Sun, J., and Tang, X., "Guided image filtering," IEEE Transactions on Pattern Analysis and Machine Intelligence **35**, 1397–1409 (2013).

[24] Pang, J., Au, O. C., and Guo, Z., "Improved single image dehazing using guided filter," (2011).